coatings

MDPI

Article

High-Temperature Tensile Behavior of an As-Cast Ni-W-Co-Ta Medium–Heavy Alloy

Yong Li [1], Yi Xiong [2,3,*], Jinjin Tang [2], Shun Han [1], Fengzhang Ren [2,3], Chunxu Wang [1] and Shubo Wang [4]

[1] Central Iron and Steel Research Institute, Beijing 100081, China
[2] School of Materials Science and Engineering, Henan University of Science and Technology, Luoyang 471023, China
[3] Collaborative Innovation Center of New Nonferrous Metal Materials and Advanced Processing Technology Jointly Established by the Ministry of Science and Technology, Luoyang 471023, China
[4] Nano and Molecular Systems Research Unit, University of Oulu, 90014 Oulu, Finland
* Correspondence: xy_hbdy@163.com

Abstract: High-temperature tensile experiments with tensile rates ranging from 0.01 s^{-1} to 10 s^{-1} were carried out at various temperatures ranging from 1000 °C to 1250 °C with a Gleeble-3800 thermal simulation tester to evaluate the physical properties of an as-cast Ni–W–Co–Ta medium–heavy alloy. The microstructure evolution of the alloy during high-temperature stretching was characterized by metallographic microscopy, scanning electron microscopy, and transmission electron microscopy. The results indicated the emergence of multiple slip lines and the parallel arrangement of dislocations in the grain of the alloy after high-temperature stretching, and typical characteristics of plane slipping were observed. The plasticity of the Ni–W–Co–Ta medium–heavy alloy increased, but its strength decreased with an increase in the deformation temperature. In contrast, an increase in the strain rate resulted in a noticeable increase in the strength and plasticity of the medium–heavy alloy. The experiments revealed that the maximum tensile strength of the as-cast Ni–W–Co–Ta medium–heavy alloy was 735 MPa (T = 1000 °C, $\dot{\varepsilon}$ = 10 s^{-1}). Additionally, the maximum reduction in area and elongation was 38.1% and 11.8% (T = 1250 °C, $\dot{\varepsilon}$ = 10 s^{-1}), respectively. The mode of fracture after high-temperature tensile deformation was brittle fracturing.

Keywords: as-cast Ni–W–Co–Ta medium–heavy alloy; high-temperature deformation; mechanical properties; brittle fracture

check for updates

Citation: Li, Y.; Xiong, Y.; Tang, J.; Han, S.; Ren, F.; Wang, C.; Wang, S. High-Temperature Tensile Behavior of an As-Cast Ni-W-Co-Ta Medium–Heavy Alloy. *Coatings* **2024**, *14*, 323. https://doi.org/10.3390/coatings14030323

Academic Editors: Giorgos Skordaris and Hideyuki Murakami

Received: 17 January 2024
Revised: 3 March 2024
Accepted: 5 March 2024
Published: 8 March 2024

1. Introduction

Tungsten heavy alloys (WHAs) are widely used in die-casting molds, counterweights, shock-absorbing devices, aerospace gyroscope rotors, and flywheels for mechanical engineering because of their high density and toughness, excessive penetration potential, and good dynamic properties [1–5]. However, their scope of use is limited because the WHAs presently in use have some shortcomings, such as a complicated fabrication process, low electrical conductivity and toughness, and excessive adiabatic shear sensitivity [6]. Therefore, much research has been carried out to enhance the overall properties of WHAs. Gong et al. [7] investigated a sintered 93W–4.9Ni–2.1Fe–0.03Y alloy subjected to speedy hot extrusion at a temperature of 1150 °C. It was proven that the dynamic recovery procedure of the 93W–4.9Ni–2.1Fe–0.03Y alloy is incomplete during a short extrusion time, and the high-density dislocations lead to intense work-hardening of tungsten alloys. After hot extrusion, the tensile strength of the alloy increased from 995 MPa in a sintered state to 1570 MPa, and the hardness increased from 29 HRC to 48 HRC. Kiran et al. [8] systematically studied the effect of tungsten content (90–95 wt%) on the mechanical properties of WHAs, and the results confirmed that the tensile strength and yield strength of WHA reached their maximum value at a tungsten content of 93%, but the elongation and impact energy decreased with an increase in the tungsten content. Prabhu et al. [9] found that

an 90W–6Ni–2Fe–2Co alloy, which was prepared by microwave sintering, exhibited an increase in tensile strength from 650 MPa under liquid phase sintering to 740 MPa, and the impact energy increased from 70 J/cm^{-2} under liquid phase sintering to 203 J/cm^{-2}. Cordero et al. [10] found that a superfine tungsten alloy with a grain size of 130 nm prepared by fast discharge plasma sintering after ball milling increased in hardness to 12 GPa and in dynamic impact strength to 4.14 GPa. From these research results, it can be seen that current studies have improved the static tensile properties and dynamic mechanical properties of WHAs to some degree. But the price of W is high, and the tungsten reserves in the world are only 3.7 million tons, restricting the bulk production and large application of WHAs [11]. Therefore, a medium–heavy alloy (MHA) with a medium W content (50%–75%) was proposed by Ye et al. [12] to reduce the costs of WHAs. It was found that MHAs and WHAs have similar mechanical properties; thus, MHAs could be used as a substitute for WHAs. And the Ni-W series alloy has been widely studied and used as hard, wear-resistant, and corrosion-resistant coatings on account of its hardness, wear resistance, and corrosion resistance [13,14]. However, conventional MHAs and/or WHAs are mainly prepared through powder metallurgy methods. The materials obtained by these methods always have faults such as porosities and weak bonding between two phases, which make it quite challenging to apply MHAs and/or WHAs in harsh service environments [15–20]. Therefore, the search for novel MHAs with excellent comprehensive mechanical properties is still ongoing [21].

A cast Ni–W–Co–Ta medium–heavy alloy was prepared through a full smelting process with nickel as the matrix of the face-centered cubic (FCC) structure and tungsten as the strengthening phase, along with other alloying elements. It possesses the characteristics of high strength and toughness, excellent dynamic performance similar to that of ultra-high-strength steel, and high density and high temperature resistance similar to those of tungsten alloys. It is a novel MHA material with excellent overall performance [22]. However, the Ni–W–Co–Ta MHA had some problems after casting, such as coarse grains, poor plasticity at high temperatures, ease of cracking during forging, etc., which seriously limit its applications in industrial production. Therefore, the high-temperature tensile behavior of an as-cast Ni–W–Co–Ta MHA was studied here, providing an experimental basis and a theoretical basis for the subsequent preparation of Ni–W–Co–Ta MHAs with better comprehensive performance.

2. Experimental Materials and Research Methods

The experimental material in this study was an as-cast Ni–W–Co–Ta MHA smelted by vacuum induction melting (VIM) + vacuum arc remelting (VAR). The ingredients of the alloy ingot are displayed in Table 1.

Table 1. Chemical ingredients of the experimental material (wt%).

Chemical Component	W	Co	Ta	Mg	C	B	Ni
Percentage (wt%)	39.5	5.04	0.99	0.0002	0.0005	0.0007	margin

An as-cast sample was cut to prepare samples with suitable dimensions for tensile testing, as shown in Figure 1, and a Gleeble 3800 tester was used to stretch the samples at a constant strain rate with deformation temperatures of 1000 °C, 1050 °C, 1100 °C, 1150 °C, 1200 °C, and 1250 °C and strain rates of 0.01 s^{-1}, 0.1 s^{-1}, 1.0 s^{-1}, and 10.0 s^{-1}. Each tensile sample was loaded into the Gleeble 3800 testing machine, heated to the required temperature, and held for 5 min to heat the material evenly before stretching. The samples were quickly water-cooled to preserve the high-temperature deformation structure of the material after being pulled apart, and the process is illustrated in Figure 2. An EVO25 tungsten filament scanning electron microscope was utilized for observing the tensile fracture at high temperatures, and the acceleration voltage was 20 kV. The metallographic specimens were prepared by wire cutting, grinding, and polishing. $CuCl_2$ (10 g), HCl (200 mL), and

C_2H_2OH (200 mL) reagents were used for metallographic corrosion. The metallographic structures were observed with an OLYMPUS PMG3 optical microscope. At the same time, slices of 5 mm × 5 mm × 1 mm were cut perpendicular to the direction of stretching. After mechanical grinding to 70 μm, the round slices with a diameter of 3 mm were washed and thinned on a Gatan 691 ion thinning instrument. The microstructures under different tensile conditions were observed by JEM-2010 transmission electron microscopy.

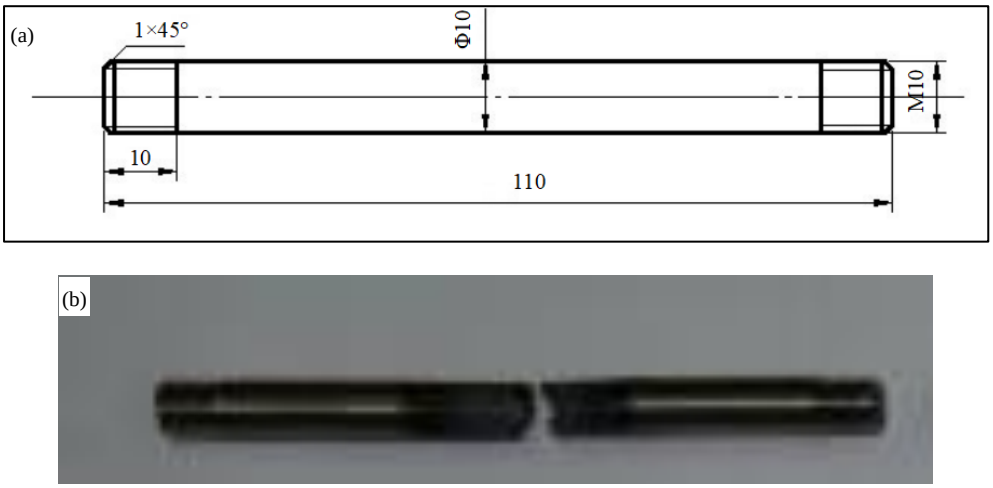

Figure 1. (**a**) Dimensions (in mm) for the thermal test of the tensile specimens and (**b**) tensile specimens after fracture.

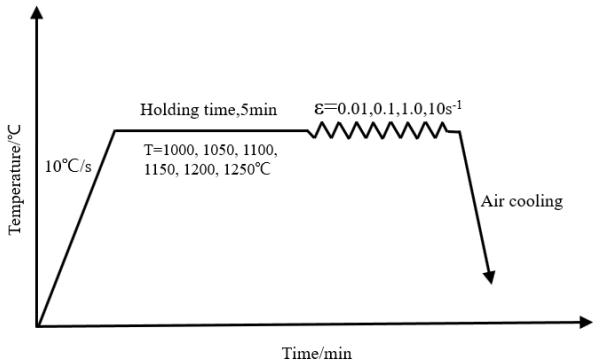

Figure 2. Thermal profile of the tensile test.

3. Experimental Results and Analysis

3.1. Analysis of the Tensile Behavior

Figure 3 shows the true stress–strain curves of the as-cast Ni–W–Co–Ta MHA at a constant strain rate under high-temperature tension. A similar trend between the stress–strain curves of the as-cast Ni–W–Co–Ta MHA at different strain rates and temperatures can be observed, in which the peak stress gradually increased with a rise in the strain rate under the same tensile temperature. This was attributed to work-hardening and, subsequently, the initiation of a large number of high-density dislocations within the alloy, and entanglement between dislocations hinders dislocation movement. The higher the deformation rate, the less likely the dynamic recovery of the alloy is to occur, so the strength of the alloy will continually increase with the deformation rate [23]. The peak stress gradually decreased with a rise in the deformation temperature under the same strain rate because the increased temperature promoted the generation of new slip systems in the alloy and the annihilation of dislocation, which reduced the density of dislocations, thus leading to a decrease in the peak stress [24]. The true stress increased sharply at the initial stage of deformation. With an increase in the strain, the growth rate of true stress slowed down and became

stable at its peak. When the strain continued to increase, the true stress decreased rapidly until it reached zero. In the initial deformation stage, massive dislocation entanglements and a dislocation mesh formed inside the as-cast Ni–W–Co–Ta alloy, resulting in a sharp increase in the density of dislocations [25]. Therefore, the deformation process of the as-cast Ni–W–Co–Ta MHA at this stage was dominated by work-hardening, resulting in a rapid increase in the true stress of the alloy. With the continued increase in the strain, the increase in the density of dislocations led to a large amount of deformation energy being stored, which drove the dynamic recovery of the alloy [26], which reduced the work-hardening effect to a certain extent. However, work-hardening still played a dominant role at this stage, so the true stress showed a stable stage after reaching its peak, which was the result of the interaction between dynamic softening and work-hardening achieving dynamic equilibrium in the material's process of deformation. Generally, the longer the duration of the dynamic equilibrium state, the greater the material's elongation, so the elongation of the as-cast Ni–W–Co–Ta MHA reached its maximum at a strain rate of 10 s^{-1}.

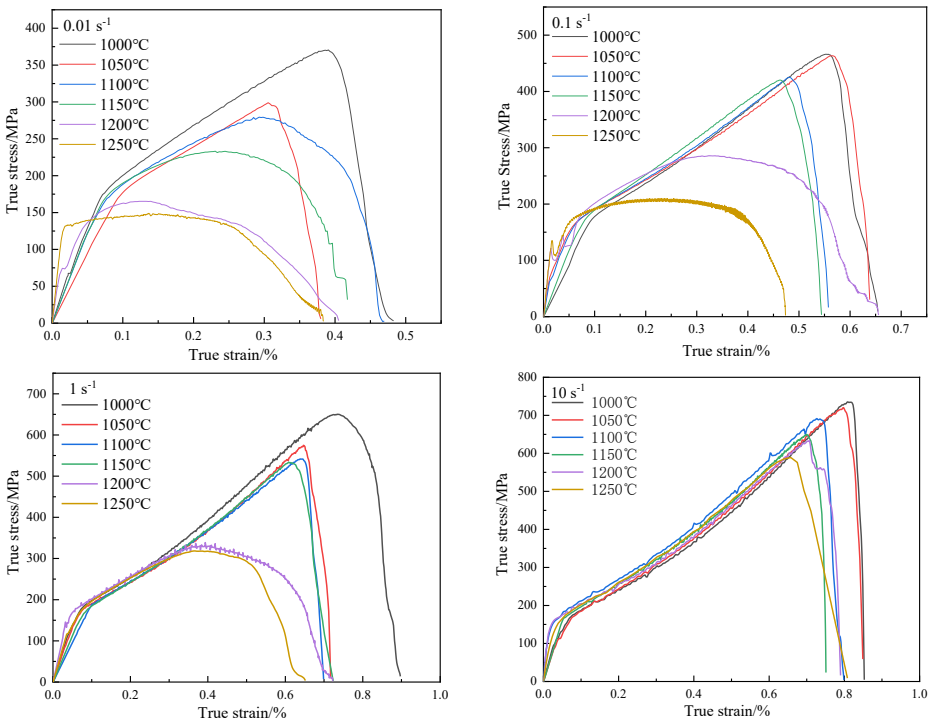

Figure 3. True stress–strain curve of the as-cast Ni–W–Co–Ta MHA after tensile deformation at high temperatures.

3.2. Metallographic Structure

Figure 4 displays the metallographic structure of the as-cast Ni–W–Co–Ta MHA before and after hot deformation. It can be seen that the grain was equiaxed, and only a small amount of undissolved particles could be observed within the grain and at the grain boundaries, as shown in Figure 4a. Previous studies on the cold deformation of Ni–W–Co–Ta MHAs have shown that the undissolved particles are composed of tungsten [21,27]. Under the tensile deformation conditions of T = 1000 °C and $\dot{\varepsilon}$ = 0.01 s^{-1}, the equiaxed grains became elongated, and a small number of voids were generated at the grain boundaries, as displayed in Figure 4b. A homogeneous phenomenon has also been found to occur in the 5A90 Al–Li alloy [28], and the reason may be that the voids generated by the as-cast alloy during tensile deformation could not be closed by means of dislocation slip and creep diffusion, so voids were generated at the grain boundaries and trinomial grain boundaries [29]. Under the same temperature, the degree of grain deformation increased significantly with a rise in the strain rate, the grains elongated into flat or long strips, and the voids generated during the stretching process gradually disappeared, as shown in Figure 4c. With a rise

in the deformation temperature (T = 1150 °C), the degree of grain deformation decreased significantly at the same strain rate, showing that the work-hardening effect of as-the cast Ni–W–Co–Ta MHA decreased, resulting in a decrease in the strength of the alloy to a certain degree, as displayed in Figure 4d.

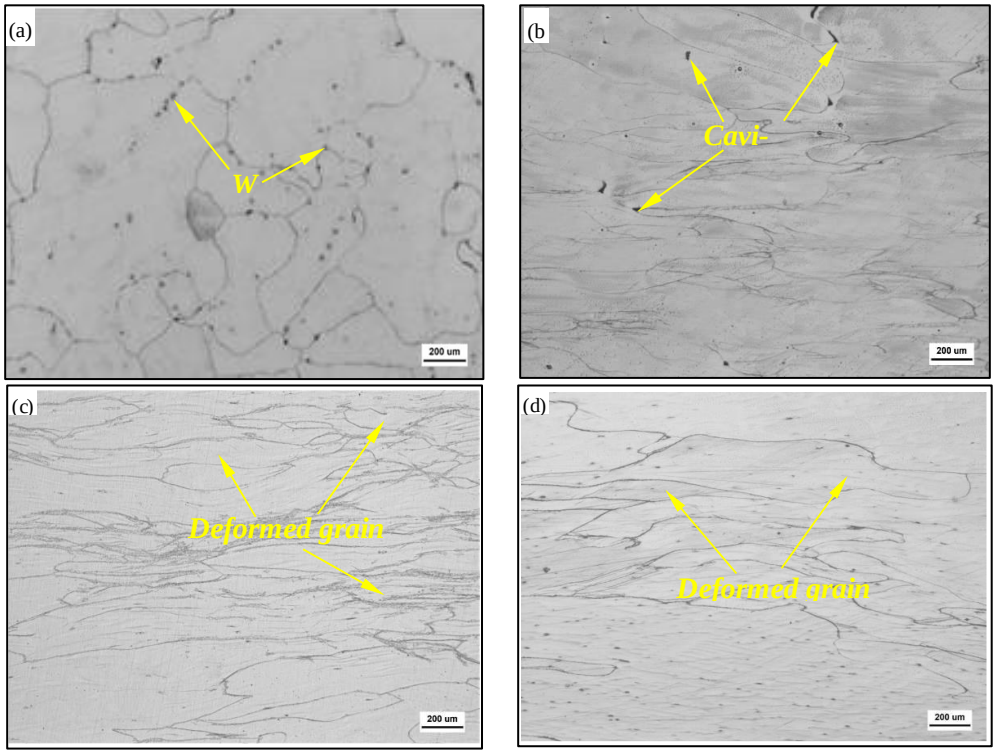

Figure 4. Metallographic structure of the as-cast Ni–W–Co–Ta MHA after high-temperature tensile deformation: (**a**) original; (**b**) 1000 °C and 0.01 s^{-1}; (**c**) 1000 °C and 10 s^{-1}; and (**d**) 1150 °C and 10 s^{-1}.

3.3. Transmission Electron Microscopy Analysis of the Microstructure

Figure 5 shows the transmission electron microscopy (TEM) images of the microstructure of the as-cast Ni–W–Co–Ta MHA after tensile deformation at the same strain rate and different temperatures. When the tensile deformation temperature was 1000 °C and the strain rate was 10s^{-1}, straight and independent dislocation lines appeared in the grain of the as-cast Ni–W–Co–Ta MHA, and the preliminary characteristics of plane slipping appeared, as shown in Figure 5a. When the tensile deformation temperature increased to 1100 °C, the dislocation structures inside the grain had a mostly parallel arrangement, and no dislocation cell structure formed. The as-cast Ni–W–Co–Ta MHA showed obvious characteristics of plane slipping. At a temperature of 1150 °C, there was no precipitation in the grains of the as-cast alloy, and it still exhibited the characteristics of planar slipping. When the tensile deformation temperature increased to 1250 °C, the dislocation of the alloy underwent dynamic recovery, resulting in a decrease in the dislocation density, which weakened the work-hardening effect during the process of tensile deformation. Therefore, the peak stress of the alloy was low under these conditions. The results showed that the internal factor controlling the wave slipping or plane slipping mode of FCC metal was the stacking fault energy [30,31]. A sample usually shows obvious characteristics of wave slipping when the stacking fault energy is high. However, planar slipping with a uniform distribution occurs when the stacking fault energy is low. The deformation mechanism of FCC metals and alloys is greatly affected by the stacking fault energy. For this as-cast Ni–W–Co–Ta MHA, although there are no relevant research results to illustrate the extent of its lamination fault energy, some studies have shown that adding W and Co elements to a Ni matrix can effectively reduce the lamination fault energy of pure Ni [32–35]. In addition, the microalloying process of Co and Ta elements in the alloy also resulted in

the formation of short-range ordered structures inside the material [36], which are the prerequisites for the formation of plane slipping in the as-cast Ni–W–Co–Ta MHA. Figure 6 is a Ni-W phase diagram. It can be seen from the diagram that the alloy would undergo second-phase precipitation at high temperatures, and this phenomenon has been observed in our previous research. The precipitation of the second phase significantly enhances the strength of the alloy but reduces its plasticity. However, no second-phase particle is found in Figure 5. In previous studies, it was found that the precipitation of the second phase in the alloy would take a long time, and no second phase precipitation occurs in a short period of time [22]. So the second phase does not need to be considered in this study.

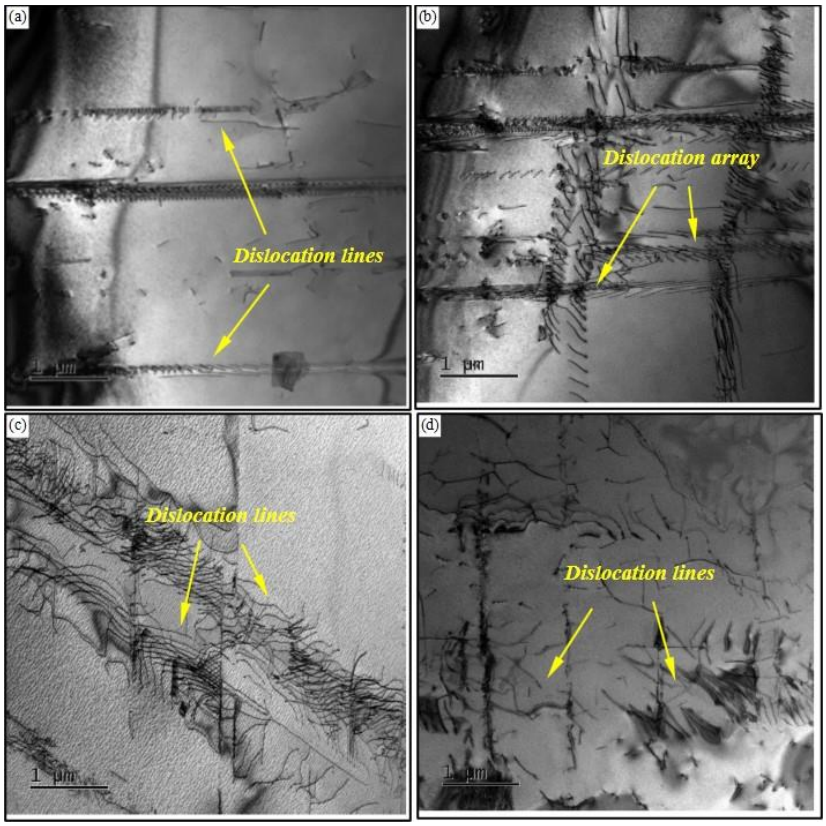

Figure 5. Microstructure of the as-cast Ni–W–Co–Ta MHA after high-temperature tensile deformation: (**a**) 1000 °C and 10 s^{-1}; (**b**) 1100 °C and 10 s^{-1}; (**c**) 1150 °C and 10 s^{-1}; and (**d**) 1250 °C and 10 s^{-1}.

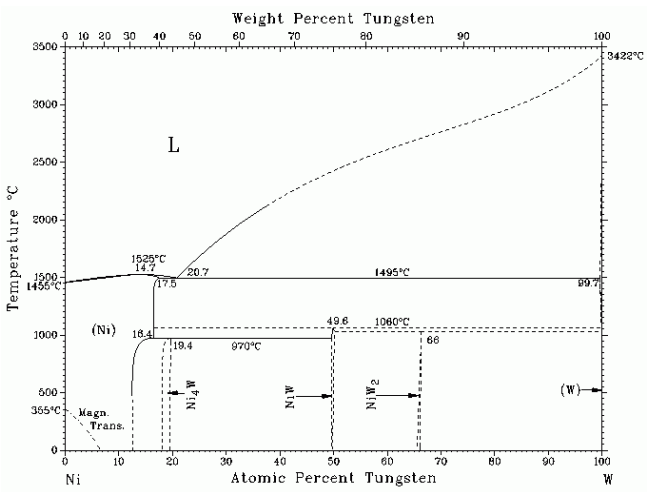

Figure 6. Ni-W phase diagram.

3.4. Mechanical Properties after High-Temperature Deformation

Figure 7 shows the changes in the mechanical properties of the high-density alloys at different deformation temperatures and strain rates. The tensile strength of the MHA decreased with an increase in the deformation temperature and a decrease in the strain rate after reaching its peak value. At a temperature of 1000 °C and a tensile deformation rate of 10 s^{-1}, the tensile strength reached a maximum value of 735 MPa, as shown in Figure 7a. The reason for this phenomenon may be the increase in the deformation temperature, which led to an increase in the concentration of vacancy saturation and atomic activity in the MHA, making dislocations more prone to migration and climbing, thereby reducing the peak stress. The alloy would thus be less likely to undergo dynamic recrystallization because of the higher density of dislocations in the alloy under the higher strain rate, so the strength of the alloy constantly increased with an increase in the strain rate [28]. In Figure 7b,c, it can be seen that the reduction in the area and elongation of the new high-density alloy reached their lowest values at 1000 °C under the same strain rate and gradually increased with an increase in the deformation temperature. This is on account of the strengthening of the amplitude within the MHA and the increase in atomic activity as the temperature increased, leading to an increase in the fluidity of the alloy, thereby enhancing its plasticity. A decrease in the strain rate was conducive to the full dynamic recovery of the development of dislocations, and the softening effect of the dynamic recovery of dislocation improved the elongation of the material. However, a decrease in the strain rate produced an increase in the high-temperature deformation time, and a small number of cavity defects will be generated in the alloy under a low strain rate, leading to a decrease in the plasticity of the material. Therefore, the reduction in the area and elongation of the Ni–W–Co–Ta MHAs were greatest at a strain rate of 10 s^{-1}. According to the relevant literature, WHAs exhibit relatively poor tensile properties at high temperatures. S. H. Islam [15] conducted high-temperature tensile mechanical property tests on traditional 95W-3.5Ni-1.5Fe and 95W-4.5Ni-0.5Co alloys. The results showed that when the two alloys were subjected to high-temperature tensile testing at 1100 °C, their strengths decreased to below 200 MPa and their elongation decreased to below 2%. It can be observed that the high-temperature mechanical properties of MHAs are significantly higher than those of WHAs prepared by traditional powder metallurgy.

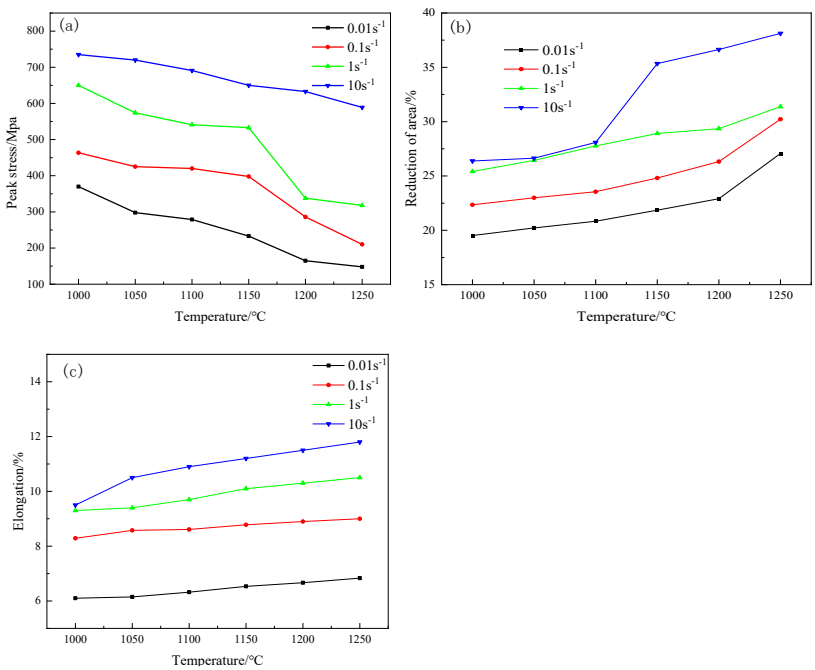

Figure 7. Mechanical properties of the Ni–W–Co–Ta MHA after high-temperature tensile deformation. (**a**) Tensile strength; (**b**) shrinkage of the area; (**c**) elongation after fracture.

3.5. Fracture Morphology

Figure 8 shows the fracture morphology of the Ni–W–Co–Ta MHA under different strain rates and temperatures. Under the conditions of T = 1000 °C and $\dot{\varepsilon}$ = 0.01 s^{-1}, the fracture morphology of the alloy is shown in Figure 8a. No obvious necking, fiber zone, or radiation zone could be observed in the MHA under these conditions. Additionally, most fractures in the plane were perpendicular to the axis of stress, exhibiting characteristics of brittle fractures, and the MHA exhibited a minimal reduction in area and elongation correspondingly. At the same temperature, as the tensile rate increased, the cross-section of the sample was mostly inclined at a 45° angle to the axis of stress. Multiple obvious holes and cracks could be observed at other sites, as well as fractures in the sample, and the fracture morphology showed typical characteristics of brittle intergranular fractures, as shown in Figure 8b. However, at the same tensile rate, with a rise in the deformation temperature, the macrofractures were relatively flat, and large cavity defects appeared. These holes are common forms of microporosity in as-cast alloys, and a local stress concentration can easily form near the holes, resulting in brittle fracturing of the alloy [37]. No obvious dimples could be observed in the fracture, and there were traces of slipping on the flat section along the edge of the crystals' section, as shown in Figure 8c. When the tensile temperature increased further, a necking phenomenon appeared at the macroscopic fracture, a certain number of cavity defects emerged at the fracture, and the reduction in area and elongation achieved optimum values. A small number of shallow dimples can be observed in the enlarged area, and the fractures were also brittle fractures, as shown in Figure 8d.

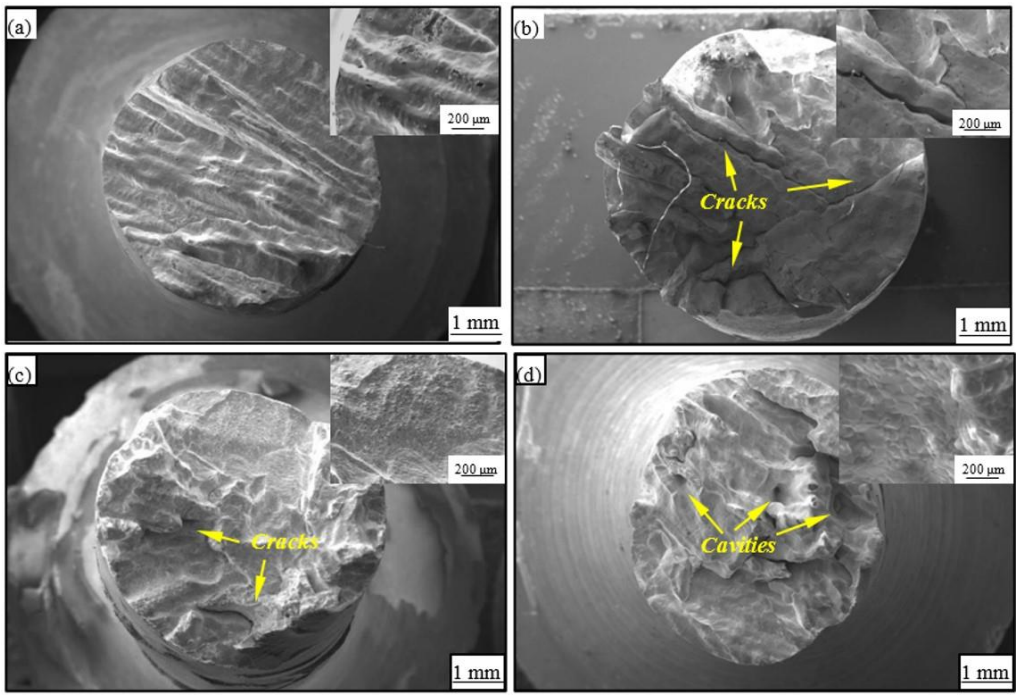

Figure 8. Fracture morphology of the as-cast Ni–W–Co–Ta MHA after high-temperature deformation: (**a**) 1000 °C and 0.01 s^{-1}; (**b**) 1000 °C and 10 s^{-1}; (**c**) 1150 °C and 10 s^{-1}; and (**d**) 1250 °C and 10 s^{-1}.

From the above results, it can be seen that the as-cast MHA maintains a certain amount of elongation during high-temperature tensile tests, but its strength is relatively low and may be limited in practical applications. Therefore, we will further improve its strength in future work to meet usage requirements.

4. Conclusions

In this study, high-temperature tensile experiments were carried out on an as-cast Ni–W–Co–Ta MHA for the first time to study its microstructure evolution and mechanical properties under different deformation temperatures and rates of strain. The following conclusions could be drawn:

(1) When the as-cast Ni–W–Co–Ta MHA was stretched at a constant strain rate, the plasticity of the as-cast Ni–W–Co–Ta MHA improved, but the strength of the alloy reduced with the tensile deformation temperature. Both the strength and plasticity of the alloy improved with an increase in the deformation rate.

(2) The as-cast Ni–W–Co–Ta MHA exhibited typical characteristics of plane slipping, with straight and independent slip lines and parallel dislocation arrays in the grain after deformation at a constant tensile strain rate.

(3) The maximum tensile strength of the Ni–W–Co–Ta alloy was 735 MPa at T = 1000 °C and $\dot{\varepsilon}$ = 10 s^{-1}, whereas the reduction in the area (38.1%) and elongation (11.8%) of the Ni–W–Co–Ta MHA alloy were highest at T = 1250 °C and $\dot{\varepsilon}$ = 10 s^{-1}. The mode of fracture was brittle fracturing.

Author Contributions: Validation, S.H.; Formal analysis, C.W.; Investigation, J.T.; Writing—original draft, Y.L.; Writing—review & editing, Y.X.; Visualization, S.W.; Supervision, F.R. All authors have read and agreed to the published version of the manuscript.

Funding: This research was funded by [National Key Research and Development Plan], grant number [2022YFB3705200]; [Major science and technology projects of Henan Province], grant number [221100230200]; [National Natural Science Foundation of China], grant number [U1804146].

Data Availability Statement: Data are contained within the article.

Conflicts of Interest: The authors declare no conflict of interest.

References

1. Pawel, Z.; Radosław, W.; Maciej, M.; Marcin, N.; Zygmunt, P. Experimental and Numerical Study on the PG-7VM Warhead Performance against High-Hardness Armor Steel. *Materials* **2021**, *14*, 3020.
2. Yuan, S.Q.; Zhang, B.Y.; Chen, Z.M.; Shang, F.J. Current situation and development of tungsten alloy materials for warhead. *China Tungsten Ind.* **2015**, *30*, 49–52.
3. Jo, M.C.; Kim, S.; Kim, D.W.; Park, H.K.; Hong, S.S.; Kim, H.K.; Kim, H.S.; Sohn, S.S.; Lee, S. Understanding of adiabatic shear band evolution during high-strain-rate deformation in high-strength armor steel. *J. Alloys Compd.* **2020**, *845*, 155540. [CrossRef]
4. Sharma, V.; Namburu, S.A.S.; Lalwani, P.; Sagar, C.K.; Gupta, A.K. Constitutive modelling and processing map analysis of tungsten heavy alloy (92.5 W-5.25Ni-2.25Fe) at elevated temperatures. *Int. J. Refract. Met. Hard Mater.* **2018**, *76*, 168–179. [CrossRef]
5. Chuvil'deev, V.N.; Nokhrin, A.V.; Boldin, M.S.; Sakharov, N.V.; Baranov, G.V.; Belov, V.Y.; Popov, A.A.; Lantsev, E.A.; Smirnova, E.S. Influence of high-energy ball milling on the solid-phase sintering kinetics of ultrafine-grained heavy tungsten alloy. *Dokl. Phys.* **2017**, *62*, 420–424. [CrossRef]
6. Kiran, U.R.; Kumar, J.; Kumar, V.; Sankaranarayana, M.; Rao, G.N.; Nandy, T. Effect of cyclic heat treatment and swaging on mechanical properties of the tungsten heavy alloys. *Mater. Sci. Eng. A* **2016**, *656*, 256–265. [CrossRef]
7. Gong, X.; Fan, J.; Ding, F.; Song, M.; Huang, B.; Tian, J. Microstructure and highly enhanced mechanical properties of fine-grained tungsten heavy alloy after one-pass rapid hot extrusion. *Mater. Sci. Eng. A* **2011**, *528*, 3646–3652. [CrossRef]
8. Kiran, U.R.; Venkat, S.; Rishikesh, B.; Iyer, V.; Sankaranarayana, M.; Nandy, T. Effect of tungsten content on microstructure and mechanical properties of swaged tungsten heavy alloys. *Mater. Sci. Eng. A* **2013**, *582*, 389–396. [CrossRef]
9. Prabhu, G.; Kumar, N.A.; Sankaranarayana, M.; Nandy, T. Tensile and impact properties of microwave sintered tungsten heavy alloys. *Mater. Sci. Eng. A* **2014**, *607*, 63–70. [CrossRef]
10. Cordero, Z.C.; Huskins, E.L.; Park, M.; Livers, S.; Frary, M.; Schuster, B.E.; Schuh, C.A. Powder-route synthesis and mechanical testing of ultrafine grain tungsten alloys. *Met. Mater. Trans. A* **2014**, *45*, 3609–3618. [CrossRef]
11. Zuo, G.; Cui, N.N.; Li, X.J.; Wen, S.B.; Zheng, H.J. Analysis and supply suggestions of mineral industry of superior metal in our country-take tungsten, antimony, rare earth as examples. *Nat. Resour. Econ. China* **2022**, *35*, 11–17+38.
12. Ye, L.; Han, Y.; Fan, J.; Du, Z. Fabrication of ultrafine-grain and great-performance W–Ni–Fe alloy with medium W content. *J. Alloys Compd.* **2020**, *846*, 156237. [CrossRef]
13. Sunwang, N.; Wangyao, P.; Boonyongmaneerat, Y. The effects of heat treatments on hardness and wear resistance in Ni–W alloy coatings. *Surf. Coat. Technol.* **2011**, *206*, 1096–1101. [CrossRef]
14. Lee, H.B. Synergy between corrosion and wear of electrodeposited Ni–W coating. *Tribol. Lett.* **2013**, *50*, 407–419. [CrossRef]

15. Li, Z.-B.; Zhang, H.; Chen, B.; Zhang, G.-H.; Chou, K.-C. Microstructure and mechanical properties of Al_2O_3 dispersed fine-grained medium heavy alloys with a superior combination of strength and ductility. *Mater. Sci. Eng. A* **2021**, *817*, 141376. [CrossRef]
16. Wu, Z.; Zhang, Y.; Yang, C.-M.; Liu, Q.-J. Mechanical properties of tungsten heavy alloy and damage behaviors after hypervelocity impact. *Rare Met.* **2014**, *33*, 414–418. [CrossRef]
17. Islam, S.H. Variation of the mechanical properties of tungsten heavy alloys tested at different temperatures. *Rare Met.* **2011**, *30*, 392–395. [CrossRef]
18. Li, Y.; Hu, K.; Li, X. Fine-grained 93W–5.6Ni–1.4Fe heavy alloys with enhanced performance prepared by spark plasma sintering. *Mater. Sci. Eng. A.* **2013**, *573*, 245–252. [CrossRef]
19. Kim, D.; Nemat-Nasser, S.; Isaacs, J.; Lischer, D. Adiabatic shearband in WHA in high-strain-rate compression. *Mech. Mater.* **1998**, *28*, 227–236. [CrossRef]
20. Senthilnathan, N.; Annamalai, A.R.; Venkatachalam, G. Microstructure and mechanical properties of spark plasma sintered tungsten heavy alloys. *Mater. Sci. Eng. A* **2018**, *710*, 66–73. [CrossRef]
21. Xiong, Y.; Shu, K.-H.; Li, Y.; Chen, Z.-G.; Zha, X.-Q.; He, T.-T.; Han, S.; Wang, C.-X. Deformation temperature impacts on the microstructure evolution and mechanical properties of a novel medium-heavy alloy (MHA). *Mater. Sci. Eng. A* **2022**, *856*, 144005. [CrossRef]
22. Li, Y.; Liu, G.Q.; Hu, X.B.; Wu, L.H.; Tan, C.W.; Dravid, V.P.; Liu, S.Z. A novel medium heavy alloy with superior quasi-static and dynamic properties. *Scr. Mater.* **2019**, *162*, 311–315. [CrossRef]
23. Jin, Y.; Lin, B.; Bernacki, M.; Rohrer, G.; Rollett, A.; Bozzolo, N. Annealing twin development during recrystallization and grain growth in pure nickel. *Mater. Sci. Eng. A* **2014**, *597*, 295–303. [CrossRef]
24. Du, S.Y.; Chen, M.H.; Xie, L.S.; Chen, C. Warm quasi-static tensile experiment and prediction of flow stress of new Al-Li alloy. *Rare Met. Mater. Eng.* **2018**, *47*, 2113–2119.
25. Sivapragash, M.; Lakshminarayanan, P.; Karthikeyan, R.; Hanumantha, M.; Bhatt, R. Hot deformation behavior of ZE41A magnesium alloy. *Mater. Des.* **2008**, *29*, 860–866. [CrossRef]
26. Qiu, P.; Wang, J.Y.; Duan, X.G.; Lin, H.T.; Chen, K.J.; Hai, T. Study on Hot Deformation Behavior and Microstructure Evolution Mechanism of AA7021 Aluminum Alloy. *Mater. Rep.* **2020**, *34*, 8106–8112.
27. Xiong, Y.; Shu, K.-H.; Li, Y.; Chen, Z.-G.; Zha, X.-Q.; He, T.-T.; Wang, S.-B. Excellent strength-ductility synergy in a ultra-high strength Ni-W-Co-Ta medium-heavy alloy by orthogonal rolling. *J. Mater. Process. Technol.* **2023**, *316*, 117968. [CrossRef]
28. Zhao, S.; Ye, L.Y.; Zhang, X.M. Inhomogeneity of superplastic deformation of 5A90 Al-Li alloy and its effect on cavity evolution. *Trans. Nonferrous Met. Soc. China* **2013**, *23*, 2125–2132.
29. Miller, D.A.; Langdon, T.G. A cavity growth diagram for high temperature creep. *Scr. Metall.* **1980**, *14*, 179–182. [CrossRef]
30. Lukas, P.; Klesnil, M. Cyclic stress-strain response and fatigue life of metals in low amplitude region. *Mater. Sci. Eng.* **1973**, *11*, 345–356. [CrossRef]
31. Mughrabi, H. On the current understanding of strain gradient plasticity. *Mater. Sci. Eng A* **2004**, *209*, 387–389. [CrossRef]
32. Dodaran, M.S.; Guo, S.; Khonsari, M.M.; Shamsaei, N.; Shao, S. A theoretical calculation of stacking fault energy of Ni alloys: The effects of temperature and composition. *Comput. Mater. Sci.* **2021**, *191*, 110326. [CrossRef]
33. Li, W.J.; Wang, C.Y. Doping effects on the stacking fault energies of the gamma phase in Ni-based superalloys. *Chin. Phys. B* **2020**, *29*, 026401. [CrossRef]
34. Yu, X.F.; Tian, S.G.; Yang, J.H. Thermodynamic calculation of the influence of W and Co on the layer fault energy of Ni alloy. *J. Mater. Metall.* **2004**, *3*, 294–297.
35. Yuan, Y.; Gu, Y.; Cui, C.; Osada, T.; Zhong, Z.; Tetsui, T.; Yokokawa, T.; Harada, H. Influence of Co content on stacking fault energy in Ni–Co base disk superalloys. *J. Mater. Res.* **2012**, *26*, 2833–2837. [CrossRef]
36. Gerold, V.; Karnthaler, H. On the origin of planar slip in f.c.c. alloys. *Acta Met.* **1989**, *37*, 2177–2183. [CrossRef]
37. Wei, J.X.; Yan, H.; Chen, R.S. Notch strength and notch fracture mechanisms of a cast Mg-Gd-Y alloy. *Mater. Sci. Eng. A* **2022**, *835*, 142668. [CrossRef]